A new HW Vir binary from the Palomar Transient Factory

PTF1 J072455.75+125300.3 - An eclipsing subdwarf B binary with a M-star companion

M. Schindewolf[1], D. Levitan[2], U. Heber[1], H. Drechsel[1], V. Schaffenroth[1,3], T. Kupfer[4], and T. Prince[2]

[1] Dr. Remeis-Observatory & ECAP, Astronomical Institute, Friedrich-Alexander University Erlangen-Nürnberg, Sternwartstr. 7, 96049 Bamberg, Germany
e-mail: markus.schindewolf@fau.de
[2] Division of Physics, Mathematics and Astronomy, California Institute of Technology, Pasadena, CA 91125, USA
[3] Institute for Astro- and Particle Physics, University of Innsbruck, Technikerstr. 25/8, 6020 Innsbruck, Austria
[4] Department of Astrophysics/IMAPP, Radboud University Nijmegen, P.O. Box 9010, 6500 GL Nijmegen, The Netherlands

ABSTRACT

We report the discovery of an eclipsing binary – PTF1 J072456+125301– composed of a subdwarf B (sdB) star ($g' = 17.2^m$) with a faint companion. Subdwarf B stars are core helium-burning stars, which can be found on the extreme horizontal branch. About half of them reside in close binary systems, but few are known to be eclipsing, for which fundamental stellar parameters can be derived. We conducted an analysis of photometric data and spectra from the Palomar 60" and the 200" Hale telescope respectively. A quantitative spectral analysis found an effective temperature of $T_{\mathrm{eff}} = 33900 \pm 350$ K, log g = 5.74 ± 0.08 and $\log(n_{\mathrm{He}}/n_{\mathrm{H}}) = -2.02 \pm 0.07$, typical for an sdB star. The companion does not contribute to the optical light of the system, except through a distinct reflection effect. From the light curve an orbital period of 0.09980(25) d and a system inclination of 83.56 ± 0.30° were derived. The radial velocity curve yielded an orbital semi-amplitude of $K_1 = 95.8 \pm 8.1$ km s^{-1}. The mass for the M-type dwarf companion is $0.155 \pm 0.020\,M_\odot$. PTF1 J072456+125301 has similar atmospheric parameters to those of pulsating sdB stars (V346 Hya stars). Therefore it could be a high-priority object for asteroseismology, if pulsations were detected such as in the enigmatic case of NY Vir.

Key words. stars: subdwarfs, binaries: eclipsing, stars: early-type, stars: evolution, stars: horizontal branch, stars: fundamental parameters, stars: individual: PTF1J072456+125301

1. Introduction

Hot subdwarf stars (sdBs and sdOs) are core helium-burning stars with thin hydrogen envelopes that are unable to sustain hydrogen shell burning (Heber 2009). This type of star dominates the population of faint blue stars at high galactic latitudes and can be found both in the old disk as well as in the halo (Ferraro et al. 1997). With regard to galaxy evolution, sdB stars play an important role because they are believed to be a dominating source for the "UV upturn phenomenon" that can be observed in elliptical galaxies and galaxy bulges (Brown et al. 1997). Subluminous B stars are identified with evolutionary models for Extreme Horizontal Branch (EHB) stars. To form an sdB star, the progenitor star has to lose almost all of its hydrogen envelope rather quickly, right at the onset of helium burning. The remaining thin part of the envelope is inert. Close binary evolution is very likely to be responsible for the mass loss on the red giant branch (RGB) that is needed to form an sdB star (Maxted et al. 2001). A significant fraction of sdB stars have composite spectra indicating the presence of a main sequence companion of F, G or K type (Ferguson et al. 1984, Stark & Wade 2003). Such binaries have long periods of several hundreds of days to more than 1000 (Vos et al. 2013). About 50 % of the known single-lined sdB stars reside in close binaries with periods less then 30 days, hosting invisible companions that are either white dwarfs or very low mass dwarfs (Maxted et al. 2001, Copperwheat et al. 2011).

To understand the formation of the sdB binaries, two possible channels have been proposed, both requiring interacting binary systems (Han et al. 2002, Han et al. 2003):

(i) The first one is called the "stable Roche lobe overflow (RLOF) channel". Stable mass transfer is taking place, originating from a low mass giant filling its Roche lobe close to the tip of the RGB. During this time it loses most of its envelope due to the Roche lobe overflow. When the hydrogen envelope has been reduced sufficiently, the mass transfer stops and the star begins to shrink. If the degenerate core is massive enough, a helium flash is possible. Subdwarf B systems originating from the RLOF channel are predicted to have long periods from 10 d up to 1000 d.

(ii) The second one is the "common envelope ejection channel" (CEEC). Again mass transfer occurs close to the tip of the red giant branch of the sdB progenitor, but the mass transfer rate is so high that a common envelope (CE) is formed. Due to friction in the envelope, both stars approach each other. This leads to a release of orbital energy and angular momentum which is used to eject the envelope. This process results in a close binary system. If the core of the initially more massive star is still able to ignite helium burning, it becomes an sdB. The result would be an sdB star with a main sequence companion in a short period binary such as the HW Vir star discussed in this paper. If a second common envelope phase occurs the companion would be a white dwarf in a close orbit to the sdB

star.

The mass distribution of sdB stars is found to peak at the canonical sdB mass of $0.47\,M_\odot$ (Dorman et al. 1993). Observational mass determinations for a few objects are consistent with such predictions ($0.47 \pm 0.031\,M_\odot$ Van Grootel et al. 2014, Fontaine et al. 2012).

Subdwarf B stars in close binary systems with low-mass dwarf companion have been known for decades (Kilkenny et al. 1978). Those companions have been discovered by means of the reflection effect in their light curves. If those systems are eclipsing, they are called HW Vir systems, named after the first discovered system (Menzies et al. 1986). They mostly have short periods around 0.1 days and a late M-type companion (which can usually only be detected by its reflection effect, caused by the high temperature difference of both components). The short period indicates that they have undergone a common envelope phase followed by a spiral-in phase. Up to now, only fifteen such systems are known (Schaffenroth et al. (2014); Schaffenroth et al. (2014b)).

The canonical mass remains valid for HW Vir systems, although being the result of binary evolution (Han et al. 2003).

Because such eclipsing binaries offer the opportunity to determine the stellar masses, detailed analyses are crucial for as many such objects as possible.

In this paper, we present observations and analysis of a new HW Vir star discovered by the Palomar Transient Factory (PTF). The PTF is a wide field survey that searches for variable sources and optical transients. It makes use of the 1.2 m Oschin Telescope at Palomar Observatory, equipped with eleven 12k × 8k CCD cameras, and the Palomar 60" telescope (Law et al. 2009). With each exposure 7.2 square-degrees are covered. In a typical night 200 square-degrees or more are observed (Levitan et al. 2011). We describe the spectroscopic and photometric observations in Sect. 2 and their analysis in Sect. 3 (spectroscopy) and Sect. 4 (photometry). In Sect. 5 we give a summary of the results from the analysis.

2. Observations

Spectroscopic and photometric data presented here were obtained at the Palomar 60" (hereafter P60) (Cenko et al. 2006) and Palomar 200" (hereafter P200) telescopes, respectively.

2.1. Spectroscopy

The spectra of PTF1 J072456+125301 (PTF0724 hereafter) were taken at the Palomar 200" telescope with the Double Spectrograph "DBSP" (Oke et al. 1982) using a low resolution (R~ 1500). The observations took place on August 10, 2010 and were scheduled to cover the entire orbit at equally distributed phases. Thirty eight spectra were collected, covering a range fom $3000\,\text{Å}$ to $11000\,\text{Å}$. The exposure time was set between $600\,\text{s}$ and $900\,\text{s}$ per spectrum to prevent orbital smearing. A grating of 600 lines/4000 mm-blaze was used at a grating angle of $27°17''$. All P200 spectra were reduced using optimal extraction (Horne 1986) as implemented in the Pamela Code (Marsh 1989), as well as the Starlink packages kappa, figaro and convert. The spectrum is readily classified as that of an sdB star, according to the strong Stark-broadened Balmer and weak helium lines.

2.2. Photometry

We obtained a total of 1,162 photometric observations of PTF0724 with the P60 over 7 nights (details of each night are in Table A.2 in the appendix. All observations were made using a g' filter and with an exposure time of 45 sec with a dead time of approximately 21 sec between exposures.

The P60 photometric observations were de-biased, flat-fielded, and astrometrically calibrated using the P60 pipeline (Cenko et al. 2006). Stars in each individual image were identified using the Sextractor Package (Bertin & Arnouts 1996) and instrumental magnitudes were measured using optimal point-spread function photometry (Naylor 1998) as implemented by the Starlink package Autophotom[1].

Calibrated light curves were calculated using the relative photometry algorithm described in the appendix of Ofek et al. (2011) and in Section 3.1 of Levitan et al. (2011). Briefly, this algorithm identifies non-varying (over the course of the observations) "calibration" stars in the field of view and minimizes the scatter of their instrumental magnitudes by adjusting the zero-point of each individual exposure. We simultaneously fit to a reference catalog (here, USNO-B 1.0) to find an absolute calibration. This minimization is calculated using an iterative, matrix-based, least-squares approach and the resulting zero-points can then be applied to the target of interest. We note that we did not utilize the de-trending features of the algorithm as described in Levitan et al. (2011) since only one telescope/instrument was used. Measurement uncertainties are calculated from a combination of the Poisson error and the fit error. However, we note that this estimate does not include systematic errors and they are thus likely under-estimated. Calculating the systematic error accurately can be done by finding the minimum scatter observed for bright stars on each exposure, but doing so requires substantially more sources than are present in the small field of view here.

The lightcurve is characterized by a strong reflection effect and primary as well as secondary eclipses. This, together with the spectral properties of the star (see 3.2), classifies PTF0724 as an HW Vir star.

The primary minimum is quite deep, with the flux descending to about 25% of the flux at phase 0.25 ($g' = 17.2^m$ at this phase-point). For further analysis the lightcurve was normalized to 1 at phase 0.25. The ephemeris was determined by fitting Gaussians to the primary eclipses via the standard Marquardt-Levenberg algorithm (Levenberg 1944). The period could be easily derived, because several lightcurves covered more than one full orbit, containing two primary minima.

The ephemeris of the primary minimum was found to be:
HJD= 2455295.64113(8) + 0.09980(25) · E
(with the eclipse number E).

3. Spectroscopic analysis

3.1. Radial velocity curve

We begin by measuring and plotting the radial velocity (RV) curve. Since the system is single-lined, the analysis is straight forward. We made use of SPAS, the Spectrum Plotting and Analysis Suite (Hirsch 2009) to determine the radial velocity for each blue spectrum (see table A1). The RVs were measured by fitting a set of mathematical functions (Gaussians, Lorentzians

---

[1] The Starlink Software Group homepage can be found at `http://starlink.jach.hawaii.edu/starlink`

and polynomials) to the spectral lines (see Fig. 2). Three functions are used to match the continuum (polynomials), the line (Lorentzians) and the line core (Gaussians), respectively and mimic the typical Voigt profile of spectral lines. The profiles are fitted to all suitable lines simultaneously using χ^2 minimization and the RV shift with respect to the rest wavelengths with the associated 1σ error is measured.

Because we find the phase shift between the primary and secondary minima is 0.5009 ± 0.001, the eccentricity of the orbit of PTF0724 must be very small (Fig. 4). Therefore we fitted a sine curve to the RVs. Fig. 1 shows the phased RV curve with the best-fit solution. All phases of the orbit are well covered. We derived a semiamplitude of K = 95.7 ± 8.1 km s^{-1} and a system velocity of γ = −26.7 ± 5.5 km s^{-1} with a bootstrapping approach using 1200 iterations. Thereby the observational data is resampled randomly and fitted again. The standard deviation of a parameter is regarded the 1-σ error of the parameter. To estimate the contribution of systematic effects to the error budget, we modified the χ^2 of the best solution by adding systematic errors in quadrature until the reduced χ^2 reached ~1.0.
The period derived from the sinusoidal fit (P=0.0976 ± 0.0042 d) is consistent with the period derived from photometry (P=0.09980(25) d) resulting in a mass function of f(m)=0.0093±0.002 M$_\odot$. The inclination of the orbit is well constrained by photometry ($i = 83.56 \pm 0.30°$, see Sect. 4). Adopting the canonical mass of 0.47 M$_\odot$ we find a mass ratio of q=0.327 ± 0.033 by making use of the mass function.

Fig. 2. Example fit to several Balmer lines of an individual spectrum, to determine the radial velocities.
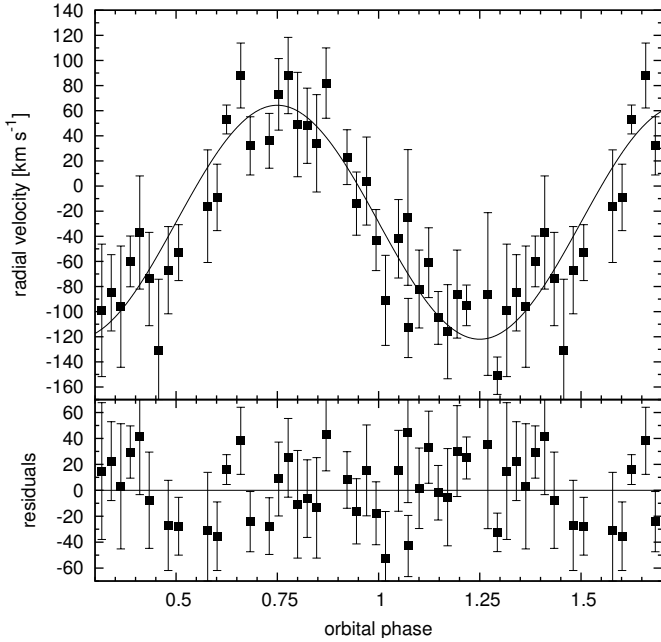

Fig. 1. Radial velocity plotted against orbital phase of PTF0724. In the bottom panel the residuals can be seen.

3.2. Atmospheric parameters

Due to the poor signal-to-noise ratio (S/N~ 10) of the individual spectra, we shifted and coadded the individual velocity-corrected spectra to improve the S/N ratio to be able to derive reliable atmospheric parameters.
Effective temperature, surface gravity and helium abundance were determined by fitting synthetic spectra to the Balmer and
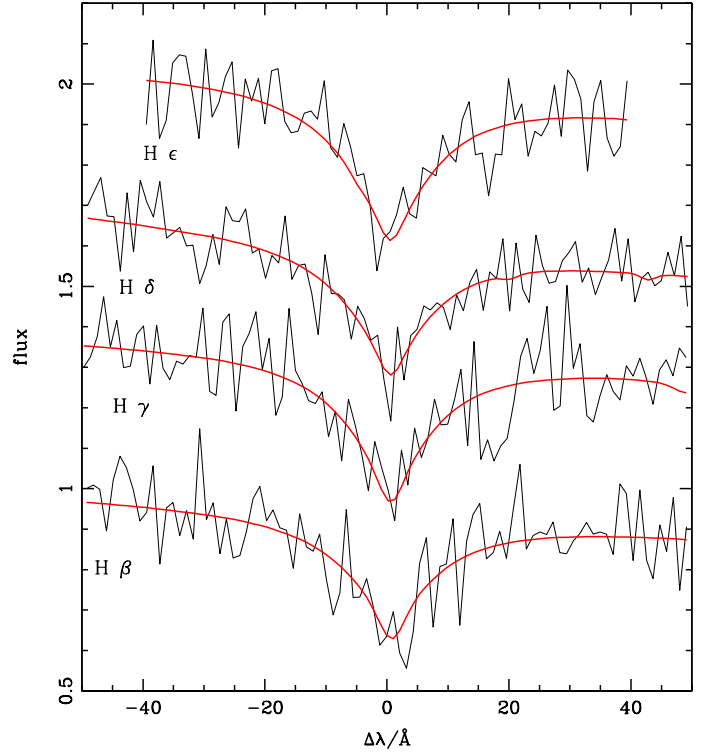
helium lines of the coadded spectra. The synthetic spectra were calculated by using LTE model atmospheres with solar metallicity and metal line blanketing (Heber et al. 2000). The derived parameters are: T$_{eff}$ = 33900 ± 350 K, log g = 5.74 ± 0.08 and log y = −2.02 ± 0.07.
The errors of the parameters were calculated with a bootstrapping approach.

In Fig. 3 the position of PTF0724 in a (T$_{eff}$, log g) diagram is compared to the known sdB+dM systems in close binary systems with known periods (Kupfer et al. 2015). Its position in the graph indicates that the primary component in PTF0724 is a normal sdB close to core helium exhaustion. Similar systems lie in the same regime. There are two classes of multi-periodic pulsating stars known among the sdB stars, which show either g-modes (361 Hya stars) or p-modes (V1093 Her stars). It is worthwhile to mention that its atmospheric parameters place PTF0724 in a regime where the driving of g-mode pulsations is predicted to be largest (Charpinet et al. 2007).

4. Lightcurve analysis

The seven lightcurves, derived from the observations in Table 2, were phased, normalized and merged into one lightcurve (see Fig.4). Its analysis proceeds as described in Drechsel et al. (2001) , for details see also Schaffenroth et al. (2013).
The LC analysis was performed by using the MORO code (MOdified ROche Program, see Drechsel et al. 1995). The program is based on the Wilson-Devinney approach (Wilson & Devinney 1971) but uses a modified Roche model that takes the radiative pressure of the stars into account. The optimization of parameters, is achieved by the *simplex* algorithm.
One of the main problems with lightcurve analysis is the large number of free parameters. For a single lightcurve 17 parameters
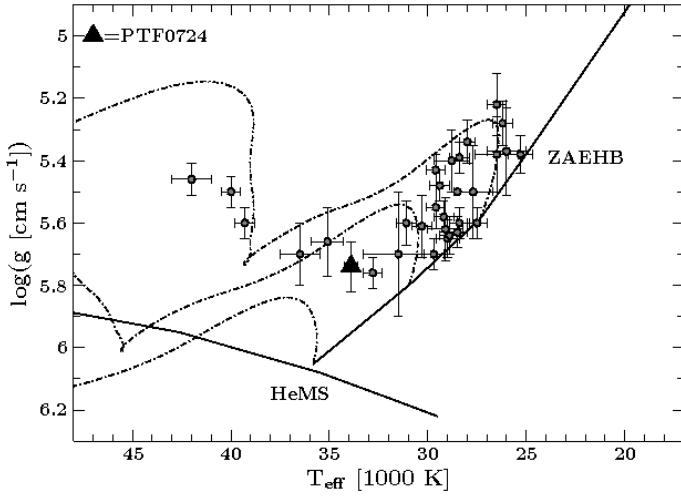
Fig. 3. Position of PTF0724 (black triangle) in a (T_{eff}, log g) diagram in comparison the known sdB+dM systems in close binary systems with known periods (grey circles, Kupfer et al. 2015). Overplotted EHB evolutionary tracks by Han et al. (2002) using 0.50 M$_\odot$ models (dashed-dotted lines). In addition the Zero-Age Horizontal Branch (ZAEHB) as well as the helium main sequence (HeMS) are shown.

have to be adjusted but parameter correlations exist. However, some of the parameters could be constrained from the spectroscopic analysis or on theoretical grounds, e.g. limb and gravity darkening parameters (see Table 1). Too many free parameters tend to generate under-determined solutions and there is no guarantee of uniqueness.

In particular the mass ratio, one of the most important solution parameters, is strongly correlated with other parameters (i.e the Roche potentials Ω) and causes a degeneracy of solutions. Therefore, in a first step, the mass ratio was fixed, while the other parameters were adjusted. Thereafter the mass ratio was changed by a certain increment and the iterative process started again.

The effective temperature and the surface gravity of the primary component were derived from the spectroscopic analysis (see Sect. 3.2). Because of its early spectral type, the gravity darkening exponent can be fixed at $g_1 = 1$, as one would expect for radiative outer envelopes (von Zeipel 1924). For the companion, we used $g_2 = 0.32$ (Lucy 1967), as expected for convective envelopes. The linear limb darkening coefficient for the primary was interpolated from the table of Wade & Rucinski (1985) and fixed at $x_1 = 0.190$. The radiation pressure parameter (Drechsel et al. 1995) of the secondary was set to zero because of the low temperature of the secondary star. That means that the effects of the radiation pressure excerted by this star are negligible. All trial runs with different sets of parameters resulted in negligible third light. Hence there is no evidence for a third body in the system, and l_3 was set to zero. We constrain the mass ratio to the range $0.29 < q < 0.36$, as indicated by the spectroscopic measurements. For each mass ratio a large grid of synthetic lightcurves was calculated to ensure that the final solution corresponds to the global minimum.

To estimate the quality of the lightcurve fit, the sum of the squared residuals of all points to the synthetic lightcurve is calculated. The solution with the smallest sum is best. We define

$$\sigma_{fit}(x) = \sqrt{\frac{n}{n-m}\frac{1}{\sum_{\nu=1}^{n}\omega_\nu}\sum_{\nu=1}^{n}\omega_\nu d_\nu^2(x)} \quad (1)$$

Table 1. Model parameters of the lightcurve solution for q=0.33

Fixed parameters:		
$T_{eff}(1)$	[K]	33900
g_1^b		1.0
g_2^b		0.32
x_1^c		0.190
A_1^a		1.0
δ_2^d		0.0
l_3^e		0.00

Fitted parameters:		
i	[°]	83.56 ± 0.3
$T_{eff}(2)$	[K]	3300 ± 300
A_2^a		1.8 ± 0.2
Ω_1^f		5.544 ± 0.20
Ω_2^f		2.885 ± 0.15
x_2^c		0.510 ± 0.05
$\left(\frac{L_1}{L_1+L_2}\right)^g$		(0.99978 ± 0.00064)
(δ_1^d)		(0.0006 ± 0.0003)

Roche radii^h:		
r_1(pole)	[a]	0.191 ± 0.011
r_1(point)	[a]	0.193 ± 0.012
r_1(side)	[a]	0.192 ± 0.011
r_1(back)	[a]	0.193 ± 0.010
r_2(pole)	[a]	0.209 ± 0.013
r_2(point)	[a]	0.227 ± 0.013
r_2(side)	[a]	0.214 ± 0.017
r_2(back)	[a]	0.223 ± 0.015

Notes.
[a] Bolometric albedo
[b] Gravitational darkening exponent
[c] Linear limb darkening coefficient; taken from Wade et al. (1085)
[d] Radiation pressure parameter, see Drechsel et al. (1995)
[e] Fraction of third light at maximum
[f] Roche potentials
[g] Relative luminosity; L_2 is not independently adjusted, but recomputed from r_2 and $T_{eff}(2)$
[h] Fractional Roche radii in units of separation of mass centres

Table 2. Adopted stellar parameters for the components of PTF0724.

PTF1J072456+125301		
i	°	83.56 ± 0.30
M_{comp}	[$M_\odot$]	0.155 ± 0.020
a	[$R_\odot$]	0.766 ± 0.041
R_{sdB}	[$R_\odot$]	0.1488 ± 0.007
R_{comp}	[$R_\odot$]	0.165 ± 0.008
log g(sdB, phot)		5.760 ± 0.015
log g(sdB, spec)		5.75 ± 0.08

as an indicator for the quality of the fit, where d_ν are the residuals, the difference between observational data and the calculated model and ω_ν are weights that can be used to increasingly consider several data points, i.e. the bottom of the primary eclipse, m is the number of start parameters for the simplex algorithm and n is the number of data points.

It was found that there is a solution for a mass ratio of q = 0.33 that reproduces the lightcurve best (see Table 1). The re-
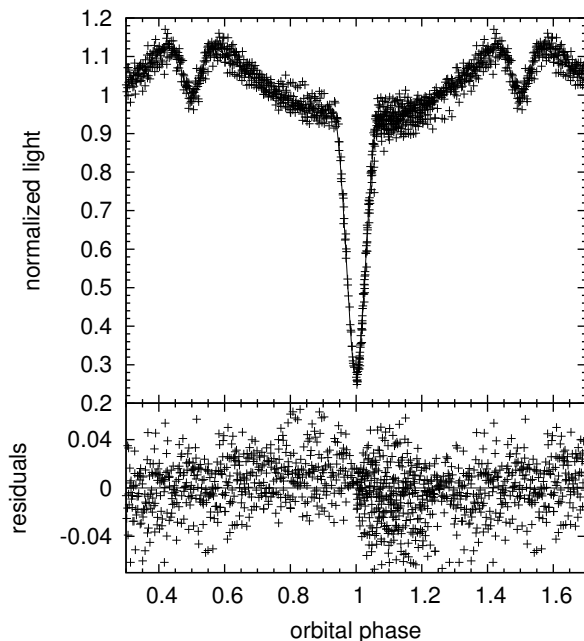
Fig. 4. Phased lightcurve of PTF0724. The solid line represents the best fitting model for q=0.33. In the bottom panel the residuals can be seen. Some outlying datapoints, mainly before and after the primary eclipse, are visible. This was most likely caused by the changing airmass. As the exact coverage of the depth and form of the bottom of the primary eclipse is crucial to get correct results, the datapoints around phase 1 were weighted higher, resulting in smaller residuals.

flection effect is dominating the shape of the lightcurve between the eclipses. No sign of ellipsoidal variations was found.

The solution requires an albedo for the companion that exceeds 1 (A2 =1.8), which means the concept of pure reflection is inadequate and reprocessing of radiation in the atmosphere of the companion has to be taken into account, which is beyond the scope of this work. An albedo exceeding unity has been found for other HW Vir systems as well (Schaffenroth et al. 2013). No reasonable fits for values of A2 =1 or less were found. Lightcurves at other wavelengths are required to better constrain the secondary's albedo.

As the reduced χ^2 for the solution is well above 1, the question arises if the errors in the photometric measurements are estimated well. If so, this could be a hint for unresolved pulsations superposed on the eclipse curve.

5. Summary

The star PTF1J072456+125301 was found to be an eclipsing binary with an orbital period of 0.09980(25) d or 2 h 23.71 min showing a strong reflection effect typical for HW Vir Stars. We obtained time series with the Palomar P60 telescope and spectroscopic data with the P200 telescope and performed an analysis of the light- and radialvelocity curves in order to pin down the systems parameters. An quantitative spectral analysis of the co-added spectrum allowed us to determine the atmospheric parameters of the sdB. The effective temperature of T_{eff} = 39000± 350 K, log(g) = 5.74±0.08 and a helium abundance of log $N_{He/H}$ = -2.02±0.07 are typical for sdB stars and place it on or near the Extreme Horizontal Branch.

From the radial velocity curve we derive the mass ratio of 0.327±0.033 by adopting the canonical sdB mass

(0.47 $M_\odot$) for the primary. The analysis of the light curve results reveal the mass, radius and temperature of the companion of M_{comp}=0.155±0.020 $M_\odot$, R_{comp}=0.165±0.015 $R_\odot$ and T_{eff}=3300±300 K, indication that the companion is a late M dwarf.

Further observations of this interesting system should be aimed at gaining spectra with better quality. High resolution spectra may reveal lines of the companion and would allow to determine the mass ratio directly from the spectra and check if there are any discrepancies with our lightcurve-based solution.

Most important would be high-quality light curves (short cadence, high signal to noise ratio), preferably in several wavebands, to search for short-period, multi-periodic light variations caused by pulsations. Their detection would make PTF0724 an ideal target for asteroseismolgy similar to the enigmatic NY Vir (Vučković et al. 2007, 2009), providing two independent tools of mass determination to be combined (Van Grootel et al. 2013).

References

Bertin, E., & Arnouts, S. 1996, A&AS, 117, 393
Brown, T.M., Ferguson, H.C., Davidsen, A.F., & Dorman, B., 1997, ApJ 482, 685
Charpinet, S. Fontaine, G., Brassard, et al., 2007, Commun. Asteroseismol. 150, 241
Cenko, S. B., Fox, D. B., Moon, D.-S., et al. 2006, PASP, 118, 1396
Copperwheat, C. M., Morales-Rueda, L., Marsh, T. R., Maxted, P. F. L., Heber, U., 2011MNRAS.415.1381C
Dorman, B.,Rood,R.T., & O'Connell, R.W. 1993, ApJ, 419,596
Drechsel, H., Haas, S., Lorenz, R., & Gayler, S. 1995, A&A, 294, 723
Drechsel, H., Heber, U., Napiwotzki, R., et al. 2001, A&A, 379, 893D
Ferguson, D. H., Green, R. F., & Liebert, J. 1984, ApJ, 287, 320
Ferraro, F., Paltrinieri, B., Fusi Pecci, F., Cacciari, C., Dorman, B., &Rood, R. 1997, ApJ 184, L 145
Fontaine, G., Brassard, P., Charpinet, S., Green, E.M., Randall, S.K., Van Grootel, V. 2012A&A...539A..12F
Han, Z., Podsiadlowski, Ph., Maxted, P. F. L., Marsh, T. R., & Ivanova, N. 2002, MNRAS, 336, 449
Han, Z., Podsiadlowski, Ph., Maxted, P. F. L., & Marsh, T. R. 2003, MNRAS, 341, 669
Heber, U., Reid, I.N., & Werner, K. 2000, A&A, 363, 198
Heber, U. 2009, ARAA, 47, 211
Hirsch, H. 2009, Phd thesis, Friedrich Alexander Universität Erlangen Nürnberg
Honeycutt, R. K. 1992, PASP, 104, 435
Horne, K. 1986, 1986PASP..98..609H
Kilkenny, D., Hilditch, R. W., &Penfold, J. E. 1978, MNRAS, 183, 523
Kupfer, T., Geier, S., Heber, U., Østensen, R. H., Barlow, B. N., Maxted, P. F. L., Heuser, C., Schaffenroth, V. Gänsicke, B. T., 2015, 2015A&A...576A..44K
Law, N.M. , 2009, 2009PASP..121.1395L
Levenberg K., Quarterly of Applied Mathematics 2: 164–168.
Levitan, D., Fulton, B.J., Groot, P.J., Kulkarni, S.R., Ofek, E.O., Prince, T.A., Shporer, A., Bloom, J.S., Bradley Cenko, S., Kasliwal, M.M., Law, N.M., Nugent, P.E., Poznanski, D., Quimby, R.M., Horesh, A., Sesar, B., Sternbarg, A., 2011, ApJ 739:68
Lucy, L. B. 1967, Zeitschrift für Astrophysik, 65, 89
Marsh, T. R. 1989, 1989PASP..101.1032M
Maxted, P. F. L., Heber, U., Marsh, T. R., & North, R. C. 2001, MNRAS, 326, 1391
Menzies, J. W., Marang, F., 1986IAUS..118..305M
Naylor, T. 1998, MNRAS, 296, 339

Ofek, E. O., Frail, D. A., Breslauer, B., et al. 2011, 2011ApJ...740...65O

Oke J. B., Gunn J. E., 1982, PASP, 94, 586

Schaffenroth, V., Geier, S., Drechsel, H., Heber, U., Wils, P, Østensen, R. H., Maxted, P. F. L., di Scala, G., 2013A&A 553A 18S

Schaffenroth, V., Geier, S., Heber, U., et al. 2014a, A&A, 564, AA98

Schaffenroth, V., Geier, S., Barbu-Barna, I., et al. 2014b, 6th Meeting on Hot Subdwarf Stars and Related Objects, 481, 253

Schaffenroth, V., Geier, S., Drechsel, H. et al. 2013, A&A, 553, A18

Stark, M. A., & Wade, R. A. 2003, AJ, 126, 1455

Van Grootel, V., Charpinet, S., Brassard, P., Fontaine, G., & Green, E. M. 2013, A&A, 553, AA97

Van Grootel, V., Charpinet, S., Fontaine, G., Brassard, P., Green, E., 2014, ASPC..481..229V

von Zeipel, H.1924, MNRAS, 84, 665

Vos, J., Østensen, R.H., Nemeth, P., Green, E.M., Heber, U., Van Winckel, H., 2013 A&A, 559,A54

Vučković, M., Aerts, C., Östensen, R., et al. 2007, A&A, 471, 605

Vučković, M., Østensen, R. H., Aerts, C., et al. 2009, A&A, 505, 239

Wade, R.A., Rucinski, S.M. 1985, A&A 60, 471

Wilson, R.E. & E.J. 1971, APJ, 166, 605

Table .1. Radial velocities with errors of PTF0724

HJD	RV in km/s		used lines	S/N (460 nm to 465 nm)
2455477.930387	-113	±15.6	Hβ, Hγ, Hδ, Hϵ	11.5
2455477.933084	-82	±23	Hβ, Hγ, Hϵ	10.7
2455477.935414	-61	±19.8	Hβ, Hγ, Hδ	9.5
2455477.937745	-105	±13.2	Hβ, Hγ, Hδ, Hϵ	10.8
2455477.940076	-116	±29.5	Hβ, Hγ, Hδ, Hϵ	11.3
2455477.942406	-86	±27.1	Hβ, Hγ, Hδ, Hϵ	11.3
2455477.944737	-95	±8.2	Hβ, Hδ, Hϵ	10.0
2455477.949969	-86	±56.8	Hβ, Hδ, Hϵ	10.4
2455477.952300	-151	±6.9	Hβ, Hγ, Hδ, Hϵ	9.9
2455477.954630	-99	±44.8	Hβ, Hγ, Hδ, Hϵ	10.0
2455477.956961	-85	±22.4	Hβ, Hγ, Hδ, Hϵ	11.7
2455477.959292	-96	±40.3	Hβ, Hδ, Hϵ	9.8
2455477.961622	-60	±12.2	Hβ, Hγ, Hδ, Hϵ	11.4
2455477.963953	-37	±37.1	Hβ, Hγ, Hδ, Hϵ	13.7
2455477.966283	-74	±29.2	Hβ, Hγ, Hδ, Hϵ	13.7
2455477.968614	-131	±48.8	Hβ, Hγ, Hδ, Hϵ	11.8
2455477.970944	-67	±26.8	Hβ, Hγ, Hδ, Hϵ	13.0
2455477.973524	-53	±14.3	Hβ, Hγ, Hδ, Hϵ	13.2
2455477.980647	-16	±36.4	Hβ, Hγ, Hϵ	14.7
2455477.982977	-9	±18.5	Hβ, Hδ, Hϵ	11.8
2455477.985308	+53	±3.5	Hγ, Hδ	13.0
2455477.988790	+88	±17.9	Hβ, Hγ, Hδ	11.9
2455477.991121	+32	±15.2	Hβ, Hγ, Hδ, Hϵ	10.2
2455477.993452	+149	±19.9	Hβ, Hγ, Hδ, Hϵ	12.5
2455477.995782	+36	±13.8	Hβ, Hγ, Hδ, Hϵ	10.0
2455477.998113	+73	±20.5	Hβ, Hγ, Hδ, Hϵ	11.2
2455478.000443	+88	±22.4	Hβ, Hγ, Hδ, Hϵ	13.4
2455478.002774	+49	±33.5	Hβ, Hγ, Hδ, Hϵ	13.2
2455478.005105	+48	±22	Hβ, Hγ, Hδ	12.3
2455478.007435	+34	±30.8	Hβ, Hγ, Hδ	11.8
2455478.009766	+82	±20	Hβ, Hγ, Hδ, Hϵ	13.4
2455478.014909	+23	±13.8	Hβ, Hγ, Hδ, Hϵ	13.7
2455478.017240	-14	±17.2	Hβ, Hγ, Hδ, Hϵ	11.2
2455478.019727	+4	±27	Hγ, Hδ, Hϵ	11.7
2455478.022058	-43	±16.3	Hβ, Hγ, Hδ, Hϵ	6.8
2455478.024389	-91	±27.9	Hδ, Hϵ	4.8
2455478.027550	-42	±23.2	Hγ, Hδ, Hϵ	6.5
2455478.029881	-25	±46.1	Hγ, Hδ, Hϵ	9.0

Table .2. Beginning and End-time of the photometric observations

Date	Begin (UTC)	End (UTC)	median seeing	# of exposures
09.04.2010	03:10:39	06:21:59	1.61"	180
08.10.2010	10:01:26	12:54:16	1.16"	164
09.10.2010	09:59:02	12:53:53	1.64"	165
10.10.2010	09:56:52	12:54:47	1.83"	167
11.10.2010	09:50:11	12:07:28	1.41"	130
13.10.2010	09:50:50	12:56:54	1.41"	176
15.10.2010	09:33:18	12:46:25	1.22"	180